

SUPPLEMENTARY MATERIAL TO
**Theoretical investigation of the molecular structure and
molecular docking of naratriptan**

WENDOLYNE LÓPEZ-OROZO¹, CLARA HILDA RIOS REYES²
and LUIS HUMBERTO MENDOZA HUIZAR^{1*}

¹Universidad Autónoma del Estado de Hidalgo, Academic Area of Chemistry, Carretera Pachuca-Tulancingo Km. 4.5 Mineral de la Reforma, Hgo, México and ²Universidad Lasalle Pachuca, Calle Belisario Dominguez 202, Centro, 42000 Pachuca de Soto, Hgo. México

J. Serb. Chem. Soc. 85 (0) (2020) 1291–1301

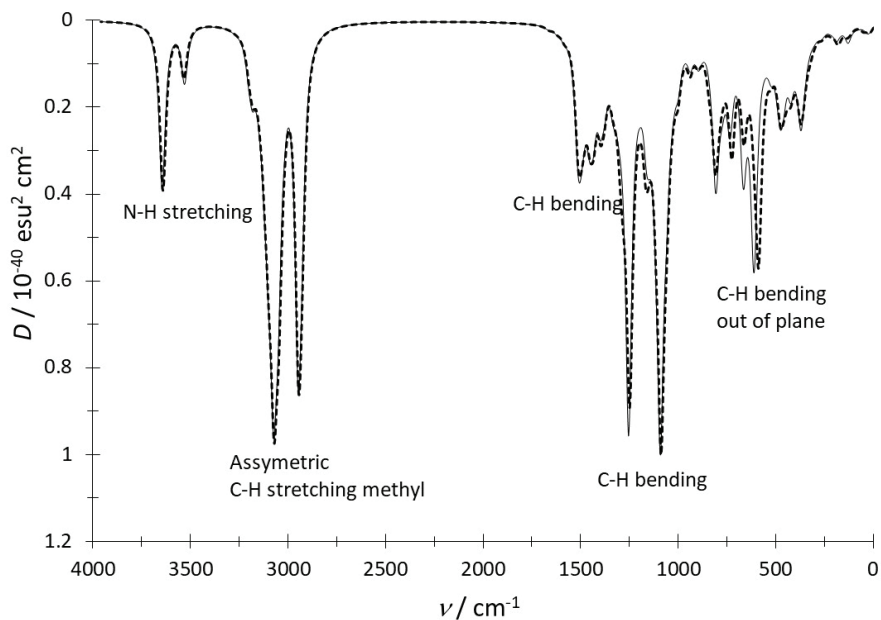


Fig. S-1. Theoretical IR spectra of Nar-I (solid line) and Nar-II (dashed line) in the aqueous phase obtained at the B3LYP/DGDZVP level of theory

*Corresponding author. E-mail: hhuizar@uaeh.edu.mx

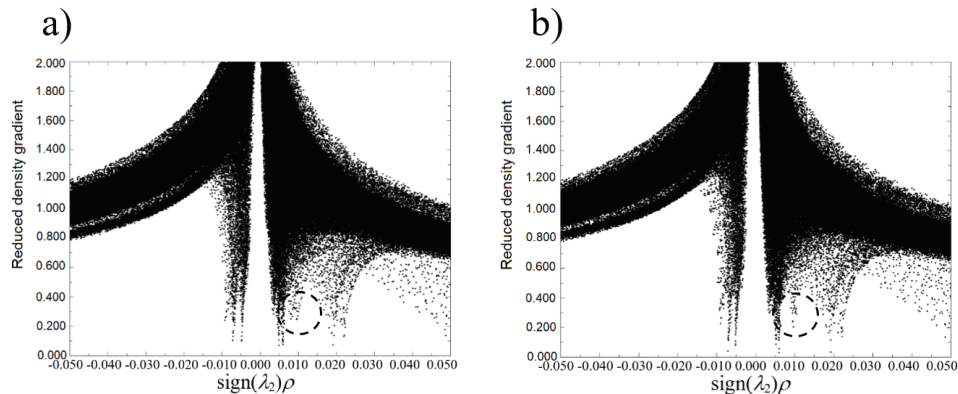


Fig. S-2. Plots of the reduced density gradient vs. $\text{sign}(\lambda_2)\rho$ for a) Nar-I and b) Nar-II. Dashed circles indicate the main differences between both plots

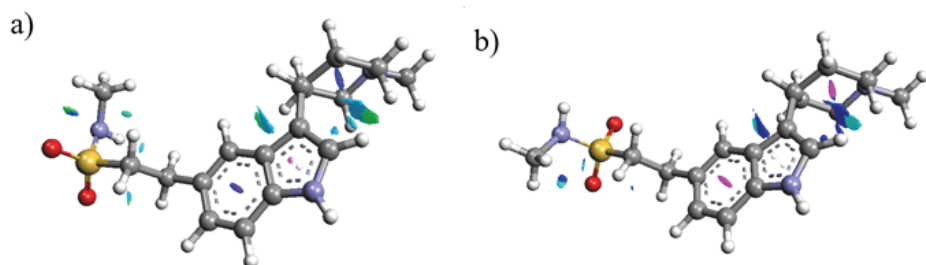


Fig. S-3. NCI Isosurfaces $\rho = 0.2$ for a) Nar-I and (b) Nar-II in the aqueous phase.

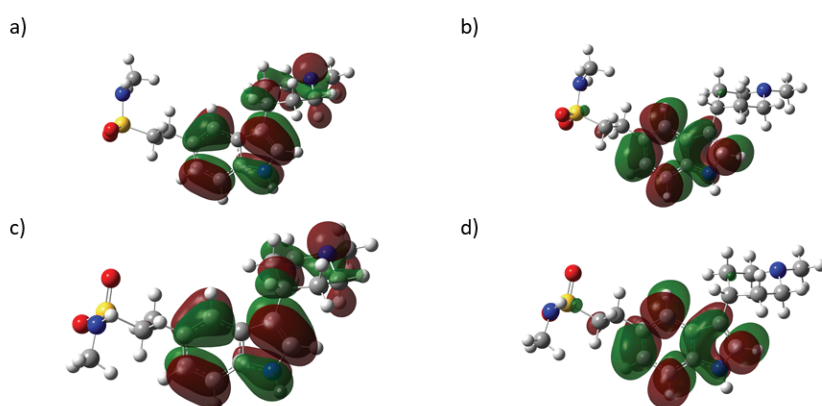


Fig. S-4. HOMO and LUMO's distributions on Nar-I and Nar-II obtained at the B3LYP/DGDZVP level of theory in the aqueous phase employing the PCM solvation model. In all cases the isosurfaces were obtained at 0.08 e/u.a.³

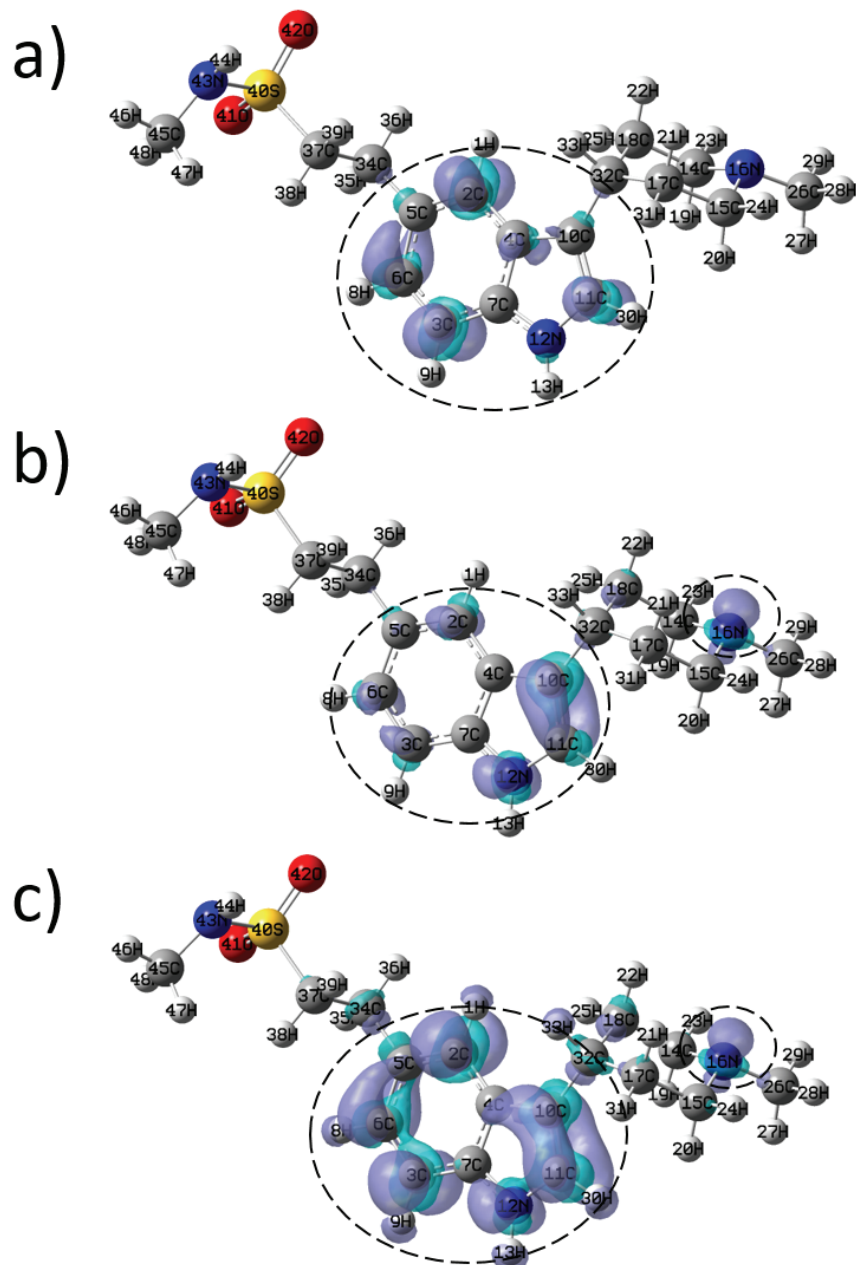


Fig. S-5. Isosurfaces of the Fukui Functions for Nar-II according to equations (10), (11) and (12) at the B3LYP/DGDZVP level of theory employing the PCM solvation model. In the case of (a) nucleophilic, b) electrophilic and c) free radical attacks. In all cases the isosurfaces were obtained at 0.004 e/u.a.³, dashed circles show the more reactive zones in each molecule.

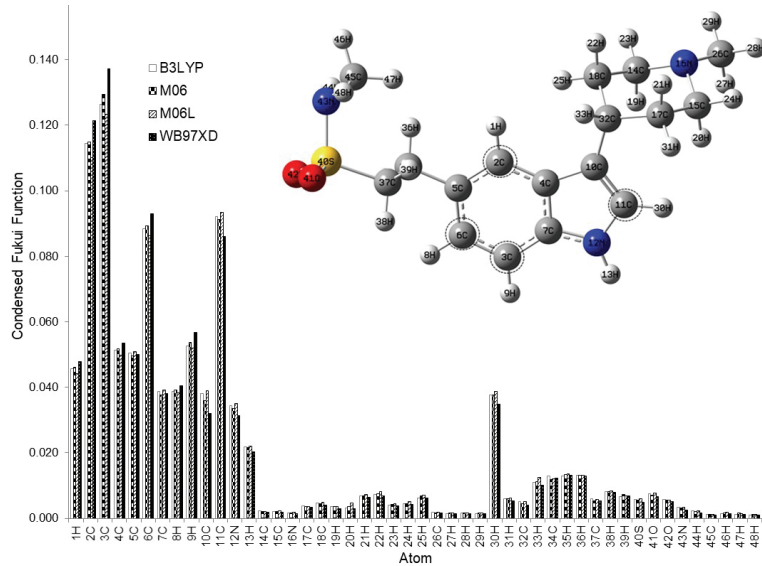


Fig. S-6. Condensed Fukui functionvalues for nucleophilic attacks on Nar-I at the X/DGDZVP (where X=B3LYP, M06, M06L and ωB97XD) level of theory, in the aqueous phase employing Hirshfeld population and equations (13)-(15), dashed circles show the more reactive zones in each molecule.

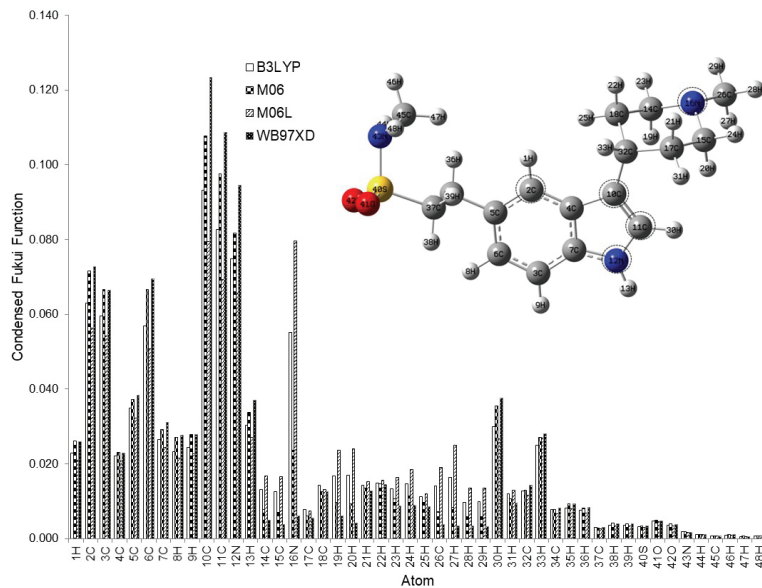


Fig. S-7. Condensed Fukui functionvalues for electrophilic attacks on Nar-I at the X/DGDZVP (where X=B3LYP, M06, M06L and ωB97XD) level of theory, in the aqueous phase employing Hirshfeld population and equations (13)-(15), dashed circles show the more reactive zones in each molecule.

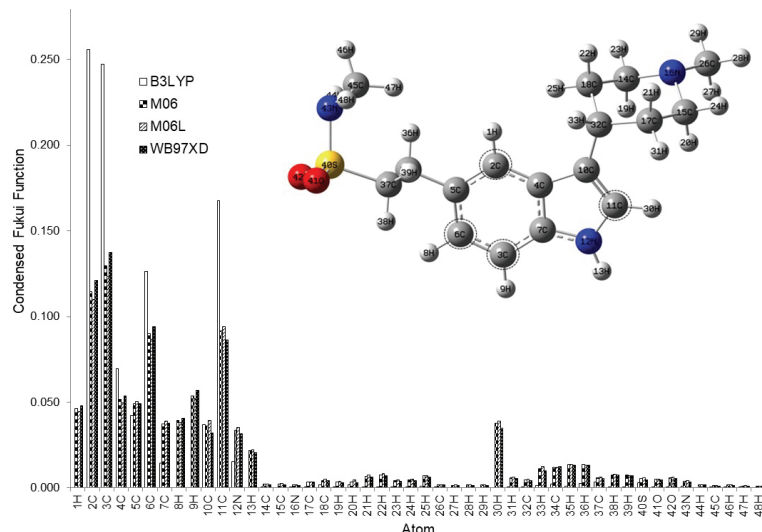


Fig. S-8. Condensed Fukui functionvalues for free radical attacks on Nar-I at the X/DGDZVP (where X=B3LYP, M06, M06L and ω B97XD) level of theory, in the aqueous phase employing Hirshfeld population and equations (13)-(15), dashed circles show the more reactive zones in each molecule.

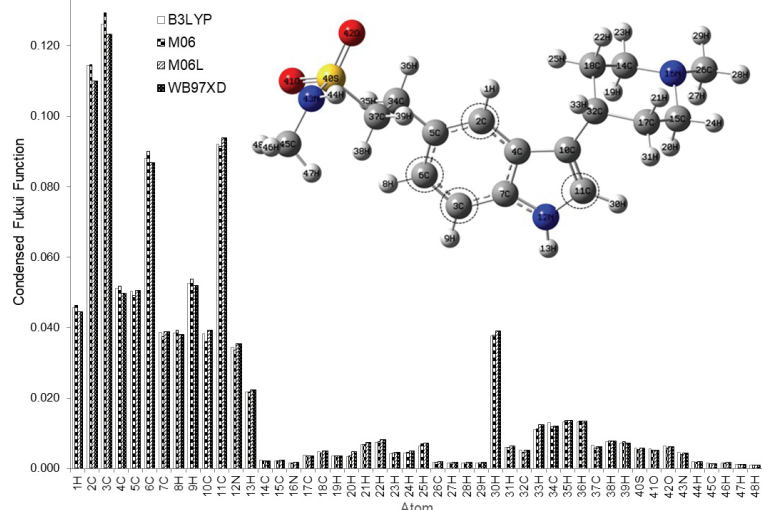


Fig. S-9. Condensed Fukui functionvalues for nucleophilic attacks on Nar-II at the X/ DGDZVP (where X=B3LYP, M06, M06L and ω B97XD) level of theory, in the aqueous phase employing Hirshfeld population and equations (13)-(15), dashed circles show the more reactive zones in each molecule.

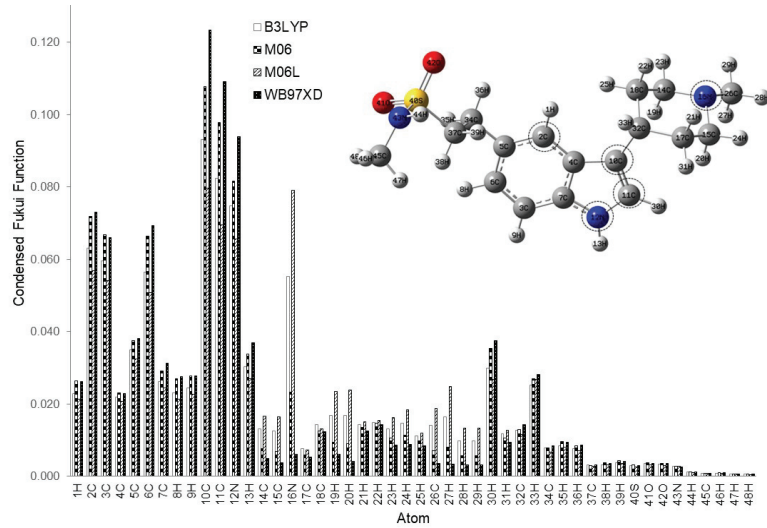


Fig. S-10. Condensed Fukui functionvalues for electrophilic attacks on Nar-II at the X/DGDZVP (where X=B3LYP, M06, M06L and WB97XD) level of theory, in the aqueous phase employing Hirshfeld population and equations (13)-(15), dashed circles show the more reactive zones in each molecule.

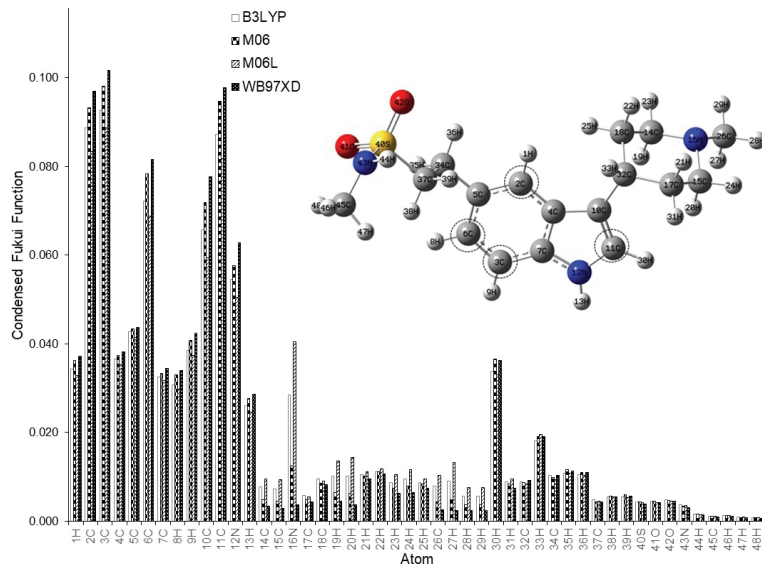


Fig. S-11. Condensed Fukui functionvalues for free radical attacks on Nar-II at the X/DGDZVP (where X=B3LYP, M06, M06L and WB97XD) level of theory, in the aqueous phase employing Hirshfeld population and equations (13)-(15), dashed circles show the more reactive zones in each molecule.

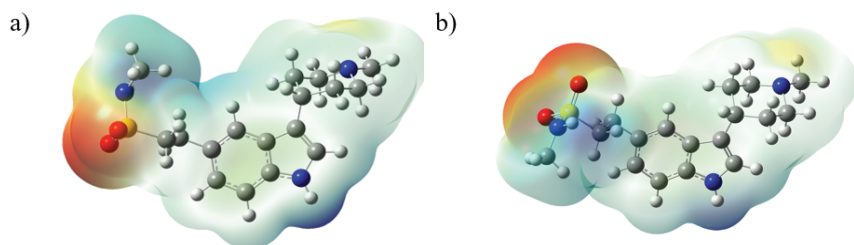


Fig. S-12. Mapping of the electrostatic potentials evaluated at the b3lyp/DGDZVP level of theory employing the PCM solvation model, onto a density isosurface (value = 0.002 e/a.u.³) for a) Nar-I, b) Nar-II.

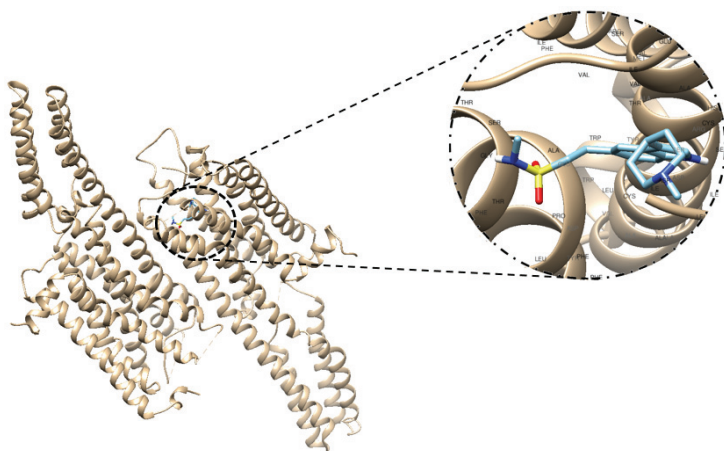


Fig. S-13. Binding site of Nar-I on the 5HT_{1B} receptor.

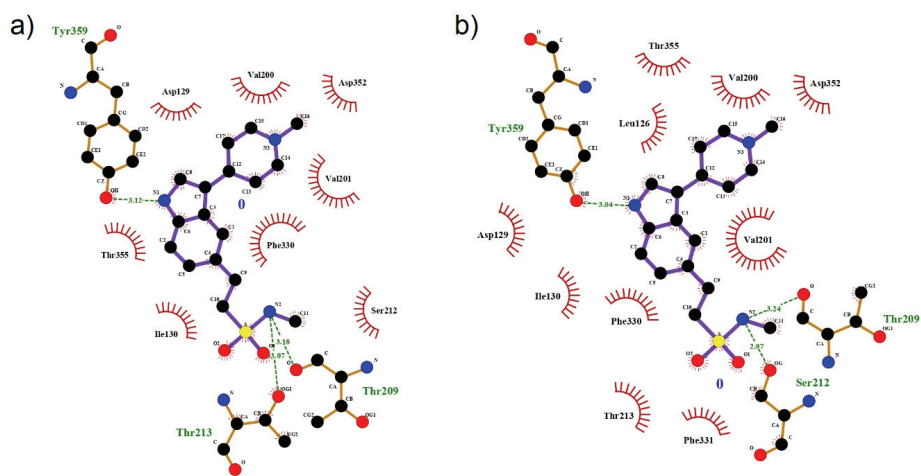


Fig. S-14. 2D ligand interaction diagram for a) Nar-I/5HT_{1B} and b) Nar-II/5HT_{1B}.